RSC Advances

PAPER

View Article Online
View Journal | View Issue

Cite this: *RSC Adv.*, 2016, **6**, 59039

Monitoring the nanostructure of a hydrogenated fullerene-like film by pulse bias duty cycle

Guangqiao Liu,[ab] Yan Zhou,[a] Bin Zhang,[a] Kaixiong Gao,[a] Li Qiang[a] and Junyan Zhang*[a]

Received 28th April 2016
Accepted 13th June 2016

DOI: 10.1039/c6ra10961f

www.rsc.org/advances

The fullerene-like (FL) nanostructure is extremely important for fullerene-like hydrogenated carbon (FL-C:H) films that exhibit excellent mechanical properties and ultralow friction in ambient air, but the details of the contributing nanostructures are not well understood. We have prepared FL-C:H films with different morphologies and contents of FL nanostructures through tailoring the pulse bias duty cycle, and have investigated the contribution of the FL nanostructures. It is found that the straighter graphitic nanostructures in FL-C:H films could form under a high pulse bias duty cycle, and the low pulse bias duty cycle could increase the five-membered ring fractions, which results in more curved FL nanostructures with a larger curvature radius. Further investigation proved that the FL nanostructures with the more curved morphology could increase the mechanical properties and improve the tribological performance of the FL-C:H films. This work established a convenient controlling method to prepare FL-C:H films with tailored structures and performance.

1. Introduction

Hydrogenated amorphous carbon (a-C:H) films have attracted increasing attention due to their extraordinary properties such as high mechanical hardness and low friction coefficients.[1,2] These properties are promising for many engineering applications, such as micro-electro-mechanical systems (MEMS) devices, space technology, journal bearings, *etc.*[3] Unfortunately, the tribological behavior of a-C:H films is extremely sensitive to the testing environment,[4–8] Therefore, it is a great challenge to fabricate lubricating carbon films with excellent mechanical properties and ultralow friction in ambient air.

Special nanostructures, such as multilayer[9,10] and composite structures[11–13] in amorphous carbon (a-C) films provide opportunities to significantly enhance the material properties at the macro scale. FL-C:H films,[14–18] named for the presence of highly curved graphitic (FL) nanostructures in an amorphous carbon matrix, have low sensitivity to the test environment[18] and have recently been the subject of extensive research. Generally, the properties of a-C:H films depend strongly on the hydrogen content and the sp^3/sp^2 hybridisation ratio,[19,20] while for FL-C:H films, the FL nanostructure is the main influence on their excellent mechanical behaviors and ultralow friction behaviors.[14–18] As is known, the characteristics and properties of carbon films are greatly affected by the deposition process, deposition parameters, the composition of reactant gases, the substrates, *etc.* The direct current (dc) magnetron sputtering of a titanium target[21,22] could be employed to produce FL-C:H films. The CVD method is another deposition technique used to prepare FL-C:H films as it has a number of advantages, such as low temperature deposition, conformal coverage of samples, good uniformity on large area substrate, and low stress for the growth of thick films. A radio frequency (RF) power supplier (as the auxiliary power)[18] and electron cyclotron resonance CVD has also been employed to deposit FL-C:H films.[23,24] We previously prepared FL-C:H films with a partial pressure ratio of 1 : 2 methane to hydrogen in a plasma enhanced chemical vapor deposition (PECVD) system by adjusting and optimizing parameters such as the gas partial pressure, the negative substrate bias, duty cycle, pulse frequency and auxiliary power,[14–16] and we found the FL nanostructure content could be adjusted by tuning the H_2 gas flows[17] or argon gas flows.[25] However, the detailed FL nanostructure contribution and the variation of possible nanostructures are not well understood. In addition, these methods are complex, time-consuming and expensive.

In previous studies,[26–28] the duty cycle is one of the most important deposition parameters that influences the microstructures and properties of films and can be modulated independently. In this work, we try to control the contribution of FL nanostructures in FL-C:H films by a pulsed direct current PECVD system using pure methane (CH_4) with a constant flow rate under a variable pulse bias duty cycle. Experimental results indicate that the contribution of FL nanostructures is in close positive relation with the pulse bias duty cycle. It is found that

[a]*State Key Laboratory of Solid Lubrication, Lanzhou Institute of Chemical Physics, Chinese Academy of Sciences, Lanzhou 730000, China. E-mail: zhangjunyan@licp.cas.cn; Fax: +86-931-4968295; Tel: +86-931-4968295*

[b]*Bailie School of Petroleum Engineering, Lanzhou City University, Lanzhou 730070, China*

the straighter graphitic nanostructures in FL-C:H films could form under a high pulse bias duty cycle, and a low pulse bias duty cycle could increase the five-membered ring fractions, which results in more FL nanostructures with a larger curvature radius. Further investigation proved that the more curved FL nanostructures could increase the mechanical properties and improve the tribological performance of FL-C:H films.

2. Experimental

2.1 Film preparation

In this study, hydrogenated carbon films were deposited on 100-oriented single crystal silicon substrates by a high frequency unipolar PECVD deposition technique. The films were about 700 nm thick and were derived from methane gas. The Si substrates were ultrasonically cleaned in acetone and alcohol sequentially for about 20 min before being transferred into the vacuum chamber. Then the substrates were treated with Ar plasma sputtering for 30 min in order to eliminate the native oxide layer on the Si surface. Subsequently, the deposition of hydrogenated carbon films was carried out at 12 sccm CH_4 flow rate at the high frequency (80 kHz) and the substrate pulsed bias voltage of −800 V for 5 h. In order to investigate the detailed contribution of the FL nanostructure, the pulse bias duty cycle was carried out from 20% to 100%.

2.2 Characterization methods

High resolution transmission electron microscopy (HRTEM) (FEI Tecnai F30, FEI, Eindhoven, The Netherlands) was carried out to study the microstructure of the as-deposited films. About 20 nm thick films grown under the above deposition conditions were produced on freshly cleaved NaCl wafers (single crystals), followed by dissolution of the NaCl substrate with distilled water and placed on Cu grids. No preparation treatments involving ion beams or chemical etching were used, which significantly reduced the possibility of introducing microstructure artifacts. Raman spectra (Jobin Yvon T64000) were collected using a 532 nm Ar laser as the excitation source. A 0.5 mW laser power was used to avoid any possible heating damage on the samples.

The mechanical properties of the as-deposited films were determined on a nanoindenter (Hysitron TriboIndenter, USA). In order to minimize the silicon substrate contribution, the indentation depth was limited to about 10% of the total film thickness. Five replicate indentations were made for each film sample. The hardness was calculated from the loading–unloading curves and the elastic recovery was calculated using the formula $(d_{max} - d_{res})/d_{max}$, where d_{max} and d_{res} are the maximum displacement at maximum load and the residual displacement after unloading, respectively.

The friction behaviors of the as-deposited films sliding against Al_2O_3 balls (diameter 5 mm, 27 GPa of hardness) were evaluated on a commercial reciprocating ball-on-disk tribometer (CSMTRIBOMETER, Switzerland). The friction tests were performed under 12 N normal loads, the amplitude is 5 mm, and the frequency is 15 Hz. All the tests were conducted in laboratory air (relative humidity ~ 40%) at room temperature (20 °C). Each sample test was repeated at least three times to acquire precise experiment results.

3. Results and discussion

The presence of FL nanostructures within carbon-based materials is normally assessed by HRTEM. Fig. 1 shows the HRTEM plane view images of the films prepared under different pulse duty cycles. It could be seen that the pulse duty cycle has an obvious effect on the contribution of the FL nanostructures. The films grown with a pulse duty cycle of 100% (namely, the direct current bias) exhibited less curved graphitic planes and more flat structures of graphene layers, where the layer spacing was about 0.34 nm and was in good agreement with the layer spacing of the graphite face (002),[29] embedded in the amorphous structures (Fig. 1(a)). As the pulse duty cycle decreased to 80%, similar nanostructures were observed in the film, but with a smaller ordering degree and shortened ordering range (Fig. 1(b)). As the pulse duty cycle was further decreased to 60%, 40%, 20% (Fig. 1(c)–(e)), there were more curved and less straight graphitic planes emerging, and these planes had large radii of curvature. These features are typical of FL arrangements.[29,30] The HRTEM results showed the formation of FL nanostructures with the low pulse duty cycle, and it is clear that the low pulse duty cycle can promote the contribution of curved graphitic structures in the films.

Raman spectroscopy can be used to further probe the microstructures of carbon films. Usually, Raman spectra of amorphous carbon films are characterized by a G peak around 1560 cm^{-1}, which is due to optical zone center vibrations (E_{2g}), a mode of pairs of sp^2 carbon atoms in aromatic rings or olefinic chains, and a D shoulder peak around 1380 cm^{-1} arising from the breathing modes of sp^2 carbon atoms in clusters of six fold aromatic rings.[31] Fig. 2 shows the Raman spectra of the as-prepared films with different pulse duty cycles. Inset shows the I_D/I_G ratio of the as-prepared films with different pulse duty cycles. Firstly, these Raman spectra showed a similar profile, however as the pulse duty cycle increased from 20% to 100%, the ratio of I_D/I_G decreased from 2.02 to 1.49 and the G peak position shifted to a slightly lower wave number, from 1568 to 1525 cm^{-1}. Also, the D shoulder peaks of the as-prepared films with different pulse duty cycles are found to be too weak, which probably indicates a significantly low proportion of defect sites in the system. These show a decrease in the sp^2 bonded carbon content in these films. Secondly, when compared with the Raman spectra of typical hydrogenated amorphous carbon films, a weak peak around 1200 cm^{-1} was present. This peak was always accompanied by the appearance of FL nanostructures, as had been confirmed by Raman spectra in FL-CN_x[32] and FL-C:H films.[16] The Raman spectrum of typical a-C:H films that could be well fitted to two Gaussian curve shapes with the D peak and G peak in the region of 1000–2000 cm^{-1}. However, the Raman spectra of these films, in addition to the peaks at 1433 and 1568 cm^{-1} of typical amorphous carbon films, can also show two extra peaks at approximately 1261 and 1506 cm^{-1} that are attributed to the curved graphite structure.[31,33] Fig. 3 shows

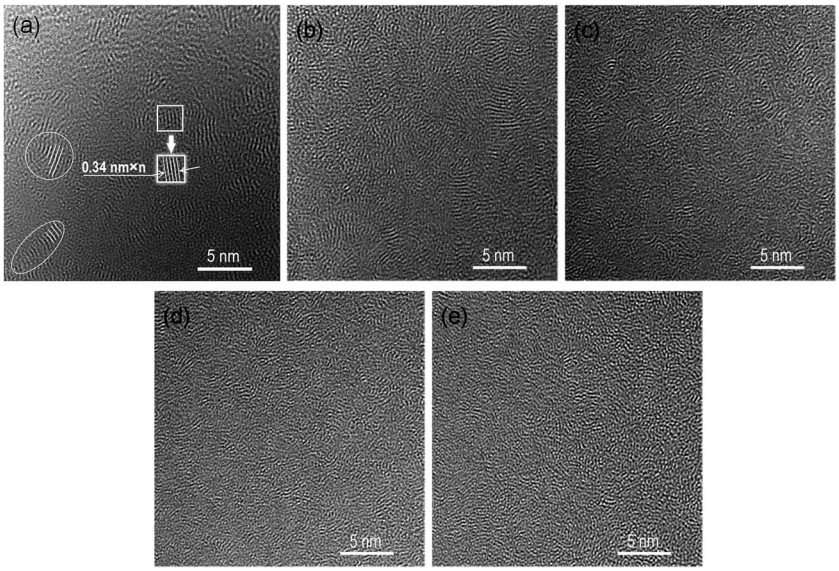

Fig. 1 HRTEM images of the as-prepared films with pulse duty cycles of (a) 100%, (b) 80%, (c) 60%, (d) 40%, (e) 20%.

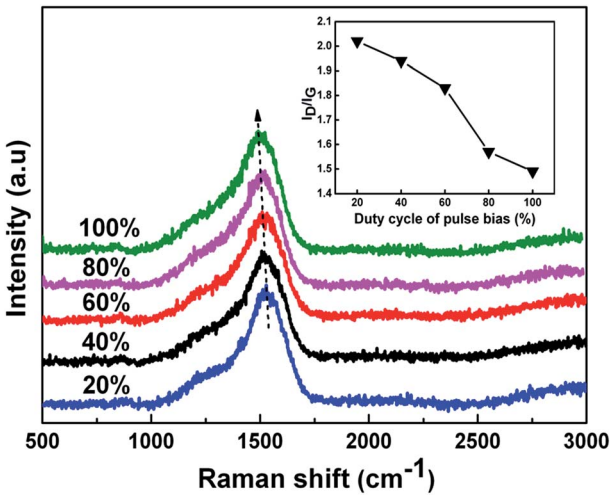

Fig. 2 Raman spectra of the as-prepared films with different pulse duty cycles. Inset shows the I_D/I_G ratio of the as-prepared films with different pulse duty cycles.

the fitted Raman spectra of the as-prepared films with pulse duty cycles of 100% and 20%. The peak at 1261 cm^{-1} originates from the seven-membered carbon rings of curved graphite, and the peak at 1506 cm^{-1} comes from the five-membered rings of curved graphite.[34–36] According to the HRTEM and Raman results above, the Raman spectrum of these films were simulated using four vibrational bands at 1261, 1433, 1506, and 1568 cm^{-1} (Fig. 3) in the region of 1000–2000 cm^{-1},[17,34,35] three with A-type symmetry (from five-, six-, and seven-membered rings) and one with E-type symmetry (from six-membered rings).

Fig. 4 shows the fractional contribution of each vibrational frequency to the Raman spectra as a function of the pulse duty cycle. The insets show the corresponding morphologies of the as-prepared films with different pulse duty cycles and the variation of the curvature (ρ_a, ρ_b, ρ_c, ρ_d, ρ_e, here $\rho = 1/r$, and r is the radii of the curved FL nanostructures) of FL nanostructures. As the pulse duty cycle increased, the fractions of $6E_{2g}$ did not show any obvious change, and the fraction of $7A_1$ was on the opposite trend to $6E_{2g}$. However, the fraction of $5A_1$ decreased monotonously and the fraction of $6A_{1g}$ changed in an inverse tendency. Moreover, as the pulse duty cycle was further increased to 60%, the fraction of $7A_1$ (0.25) in 60% pulse duty cycle had been relatively higher than the fraction of $5A_1$ (0.22) in the same pulse duty cycle. For pure carbon structures, the curvature and interlinking in purely sp^2-bonded structure can all take place through randomly oriented pentagonal and heptagonal rings or "defects" according to the atomic modeling[37] and "squeezed chicken wire" model.[38] That is to say, the decrease or increase of the fraction of five-membered rings indicates the less or more curved graphite sheets and FL nanostructures. In addition, more five-membered ring fractions of the low pulse duty cycle develop larger ring clusters due to π-bonded fraction increases, without forming layered graphite like structures, and must develop curvature to maintain a high degree of atomic packing.[39] These are in good agreement with the HRTEM results which show more curved and less straight graphitic planes, and these planes had large radii of curvature in the films with the low pulse duty cycle.

We analyzed the changes in the morphology of FL nanostructures by considering the effect of bombardment aroused by the energetic ions. Generally, ions with high energy damage the sp^3 sites and transfer sp^3 sites into sp^2 sites by ion implantation-induced irradiation damage effects,[40] and the increased duty cycle tends to release excess energy to drive local metastable sp^3 sites to form thermodynamically stable sp^2 sites.[41] So the combination of high energy ions under increased an duty cycle result in a preponderance of small, isolated clusters of six-membered rings which are both thermodynamically stable and planar in geometry[36] (as shown in

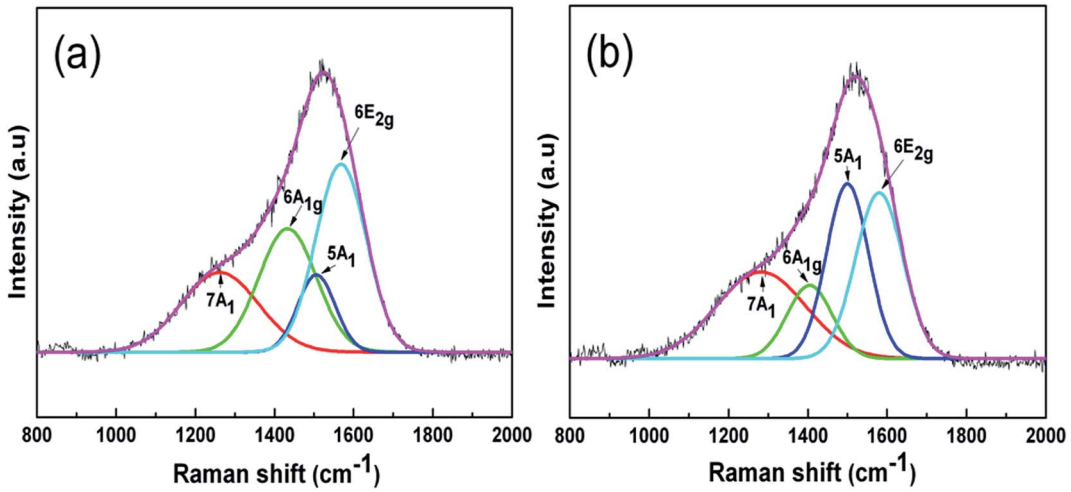

Fig. 3 The fitted Raman spectra of the as-prepared films with pulse duty cycles of (a) 100%, (b) 20%.

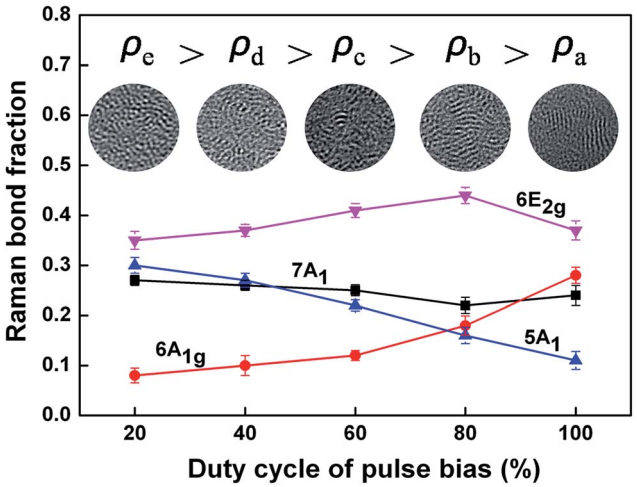

Fig. 4 Contribution to the carbon Raman band from the vibrations of five-, six-, and seven-membered rings *versus* the pulse duty cycle. Inset shows the corresponding morphologies of as-prepared films with different pulse duty cycles and the variation of the curvature (ρ_a, ρ_b, ρ_c, ρ_d, ρ_e, here $\rho = 1/r$, and r is the radii of the curved FL nanostructures) of FL nanostructures.

Fig. 1(a)). A lower pulse duty cycle corresponds to less ion bombardment and lower growth compressive stress, giving rise to the development of larger ring clusters. Meanwhile, local bonding environments exist within considerable strain fields due to the bombardment of sufficiently energetic ions that will drive plane curvature in an otherwise six-membered ring structure, resulting in the evolution of both five- and seven-membered rings. In thermodynamics, five-membered ring structures are more stable than seven membered rings.[39,42] The five-membered ring fraction consequently increases with the decrease in duty cycle. This does not mean that the six-membered ring fraction is decreasing, it only means that newly formed π-bonds are grouping into five-membered rings (as shown in Fig. 4). Furthermore, the growth process of the films results from a balance between the plasma species (hydrocarbon ions and neutrals) incident on the growing films and the film etching by atomic hydrogen.[43] The longer annealing time[27,44] with the lower pulse duty cycle guarantees the transformation of FL nanostructures, and the effective removal of hydrogen is beneficial for the formation of FL nanostructures since the effect of atomic hydrogen etching can be decreased (as shown in Fig. 1(c)–(e)).

Fig. 5 shows XPS C 1s peaks of the as-prepared films with different pulse duty cycles. The C 1s binding energies of pure graphite (284.3 eV) and diamond (285.3 eV) measured at the same conditions were cited for comparison. It could be seen that the C 1s core positions of the films grown with the low pulse duty cycles were more adjacent to the C 1s position of graphite, indicating that the films grown with the low pulse duty cycle had a higher sp^2 content and further proved that the films had more FL nanostructures.

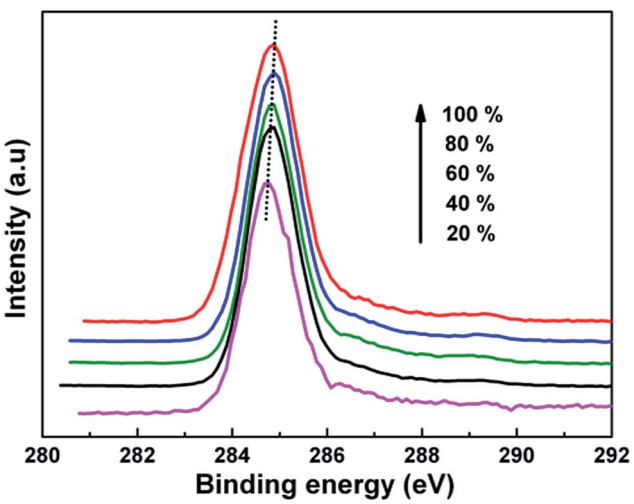

Fig. 5 XPS C 1s peaks of the as-prepared films with different pulse duty cycles.

Generally, the hardness of diamond like carbon films was linked to the presence of sp^3 C–C bonds.[45] However, for FL-C:H films, FL nanostructures consisting of bent, cross-linked, and frequently intersecting carbon sheets is key for the enhancement of the material properties at macro scale.[14–18] The mechanical properties of the as-prepared films in terms of hardness, elastic recovery under pulse duty cycles were measured by a nanoindenter. Fig. 6 shows the hardness and elastic recovery of the as-prepared films as a function of the pulse duty cycle. The inset shows the growth rate of the as-prepared films with different pulse duty cycles. By increasing the pulse duty cycle, both the hardness and elastic recovery of the films were lowered. The film deposited with a pulse duty cycle of 20% possess an elastic recovery as high as 87% and a hardness as high as 27 GPa. Although the film deposited with 100% pulse duty cycle shows low hardness and elastic recovery of 15 GPa and 80%, it is still clearly better than a-C:H films with a general elastic recovery of about 65% and a hardness of about 11 GPa.[16] In addition, it is found that the films with more curved and less straight FL nanostructures exhibited a lower growth rate. Apart from the HRTEM, Raman and XPS results, the mechanical properties were in close positive relations with the content and morphology of FL nanostructure generation in hydrogenated carbon films.

Fig. 7 shows the friction coefficients of the as-prepared films with different pulse duty cycles as a function of sliding times. It is clear that the friction behaviors of the films depend strongly on the pulse duty cycle. All the films exhibit a low and stable friction coefficient after the run-in stage, which is typical for the FL-C:H films in ambient conditions. With the decrease in the pulse duty cycle, a lower and more stable friction coefficient occurs. In summary, the films with more curved FL nanostructures exhibited lower friction. Especially when the pulse duty cycle decreased to 20% and the friction coefficient of the films with the most five-membered ring fraction and the largest radii of FL nanostructure curvature, reached as low as about 0.012 in air. These results provide strong evidence to support the concept that ultralow friction of FL-C:H films is in close positive relations with the content and morphology of FL nanostructure.

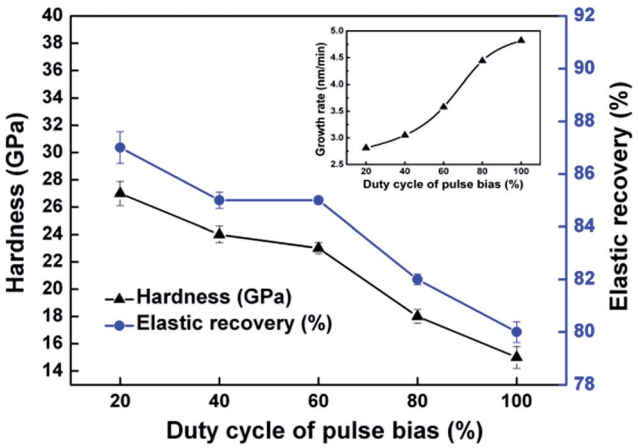

Fig. 6 Hardness and elastic recovery of the as-prepared films with different pulse duty cycles. Inset shows the growth rate of the as-prepared films with different pulse duty cycles.

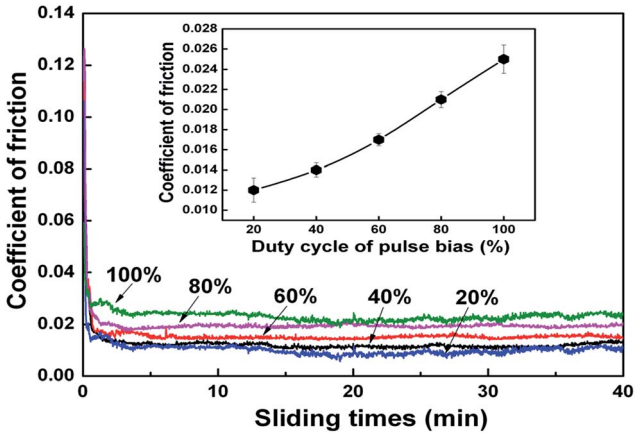

Fig. 7 Friction coefficient of the as-prepared films with different pulse duty cycles as a function of sliding times in the same test environment. Inset shows the comparison diagram of the friction coefficient.

4. Conclusion

We have prepared FL-C:H films with different contents and morphologies of FL nanostructure by varying the pulse duty cycle. The HRTEM and Raman spectrum results show that with the decrease of the pulse duty cycle from 100% to 20%, the more curved and less straight graphitic nanostructures appear in an amorphous carbon matrix and then there is an obvious increase in the amount of more curved FL nanostructures. Moreover, the mechanical properties of these films also depend on the pulse duty cycle, in which the hardness and the elastic recovery decrease with the increase of pulse duty cycle. As a consequence, the variation of pulse duty cycle also influences the tribological performances of the films, in which the lower pulse duty cycle is more beneficial for the lower friction coefficient. These results reveal that it is possible, by adjusting the pulse duty cycle, to control the FL nanostructure contribution of the FL-C:H film and further obtain quality FL-C:H films with good mechanical and tribological properties. This work establishes a method to control the FL nanostructure contribution by adjusting the pulse duty cycle, and further to obtain quality FL-C:H films with good mechanical and tribological properties.

Acknowledgements

This work was supported by the Major State Basic Research Development Program of China (973 Program) (No. 2013CB632304), National Natural Science Foundation of China (No. 51275508), the China Postdoctoral Science Foundation (No. 2013M540781), the Natural Science Foundation of Gansu Province (No. 145RJZA085).

References

1 C. Donnet and A. Erdemir, *Tribol. Lett.*, 2004, **17**, 389–397.
2 R. Maboudian, W. R. Ashurst and C. Carraro, *Tribol. Lett.*, 2002, **12**, 95–100.
3 J. Andersson, R. A. Erck and A. Erdemir, *Wear*, 2003, **254**, 1070–1075.
4 H. I. Kim, J. R. Lince, O. L. Eryilmaz and A. Erdemir, *Tribol. Lett.*, 2006, **21**, 51–56.
5 J. Andersson, R. A. Erck and A. Erdemir, *Surf. Coat. Technol.*, 2003, **163–164**, 535–540.
6 A. Erdemir and C. Donnet, *J. Phys. D: Appl. Phys.*, 2006, **39**, 311–327.
7 M. Sedlacek, B. Podgornik and J. Vizintin, *Mater. Charact.*, 2008, **59**, 151–161.
8 H. Li, T. Xu, C. Wang, J. Chen, H. Zhou and W. Liu, *Appl. Surf. Sci.*, 2005, **249**, 257–265.
9 I. J. W. Ager II, S. Anders, I. G. Brown, M. Nastasi and K. C. Walter, *Surf. Coat. Technol.*, 1997, **91**, 91–94.
10 N. Dwivedi, S. Kumar, Ishpal, S. Dayal, Govind, C. M. S. Rauthan and Q. S. Panwar, *J. Alloys Compd.*, 2011, **509**(4), 1285–1293.
11 D. Sarangi, R. Sanjinés and A. Karimi, *Carbon*, 2004, **42**(5–6), 1107–1111.
12 V. Singh, V. Palshin, R. C. Tittsworth and E. I. Meletis, *Carbon*, 2006, **44**(7), 1280–1286.
13 A.-Y. Wang, K.-R. Lee, J.-P. Ahn and J. H. Han, *Carbon*, 2006, **44**(9), 1826–1832.
14 C. Wang, S. Yang, Q. Wang, Z. Wang and J. Zhang, *Nanotechnology*, 2008, **19**, 225709.
15 Z. Wang, C. Wang, B. Zhang and J. Zhang, *Tribol. Lett.*, 2011, **41**, 607–615.
16 Q. Wang, C. Wang, Z. Wang, J. Zhang and D. He, *Appl. Phys. Lett.*, 2007, **91**, 141902.
17 Y. Wang, J. Guo, K. Gao, B. Zhang, A. Liang and J. Zhang, *Carbon*, 2014, **77**, 518–524.
18 L. Ji, H. Li, F. Zhao, W. Quan, J. Chen and H. Zhou, *J. Phys. D: Appl. Phys.*, 2010, **43**, 015404.
19 P. Koidl, C. Wild, B. Dischler, G. Wagner and M. Ramsteiner, *Mater. Sci. Forum*, 1990, **52–53**, 41–70.
20 D. Liu, B. Chen and Y. Liu, *Plasma Sci. Technol.*, 2006, **8**, 285–291.
21 P. Wang, X. Wang, W. Liu and J. Zhang, *J. Phys. D: Appl. Phys.*, 2008, **41**, 085401.
22 X. Wang, P. Wang, S. Yang and J. Zhang, *Wear*, 2008, **265**, 1708–1713.
23 J. G. Buijnsters, M. Camero, R. Gago, A. R. Landa-Canovas, C. Gómez-Aleixandre and I. Jiménez, *Appl. Phys. Lett.*, 2008, **92**, 141920.
24 J. G. Buijnsters, M. Camero, L. Vázquez, F. Agulló-Rueda, R. Gago, I. Jiménez, C. Gómez-Aleixandre and J. M. Albella, *Diamond Relat. Mater.*, 2010, **19**, 1093–1102.
25 J. Guo, Y. Wang, H. Liang, A. Liang and J. Zhang, *Appl. Surf. Sci.*, 2016, **364**, 288–293.
26 X. Dong, Z. Wu, X. Xu, T. Wang and Y. Jiang, *Vacuum*, 2014, **104**, 97–104.
27 L. Ji, H. Li, F. Zhao, W. Quan, J. Chen and H. Zhou, *J. Appl. Phys.*, 2009, **105**, 10611.
28 M. Pohler, R. Franz, J. Ramm, P. Polcik and C. Mitterer, *Surf. Coat. Technol.*, 2015, **282**, 43–51.
29 J. Neidhardt, L. Hultman and Z. Czigány, *Carbon*, 2004, **42**, 2729–2734.
30 I. Alexandrou, C. J. Kiely, A. J. Papworth and G. A. J. Amaratunga, *Carbon*, 2004, **42**(8–9), 1651–1656.
31 A. C. Ferrari and J. Robertson, *Phys. Rev. B: Condens. Matter Mater. Phys.*, 2000, **61**, 14095.
32 C. Wang, S. Yang, H. Li and J. Zhang, *J. Appl.Phys.*, 2007, **101**, 013501.
33 J. Schwan, S. Ulrich, V. Batori, H. Ehrhardt and S. R. P. Silva, *J. Appl. Phys.*, 1996, **80**, 440.
34 T. E. Doyle and J. R. Dennison, *Phys. Rev. B: Condens. Matter Mater. Phys.*, 1995, **51**, 196.
35 M. P. Siegal, D. R. Tallant and L. J. Martinez-Miranda, *Phys. Rev. B: Condens. Matter Mater. Phys.*, 2000, **61**, 10451.
36 M. P. Siegal, P. P. Provencio, D. R. Tallant, R. L. Simpson, B. Kleinsorge and W. I. Milne, *Appl. Phys. Lett.*, 2000, **76**, 2047–2049.
37 S. J. Townsend, T. J. Lenosky, D. A. Muller, C. S. Nichols and V. Elser, *Phys. Rev. Lett.*, 1992, **69**, 921.
38 I. Alexandrou, H. J. Scheibe, C. J. Kiely, A. J. Papworth, G. A. J. Amaratunga and B. Schultrich, *Phys. Rev. B: Condens. Matter Mater. Phys.*, 1999, **60**, 10903.
39 M. P. Siegal, D. R. Tallant, P. N. Provencio, D. L. Overmyer and R. L. Simpson, *Appl. Phys. Lett.*, 2000, **76**, 3052.
40 T. Xu, S. Yang, J. Lu, Q. Xue, J. Li, W. Guo and Y. Sun, *Diamond Relat. Mater.*, 2001, **10**, 1441–1447.
41 A. Liu, J. Zhu, J. Han, H. Wu and Z. Jia, *Appl. Surf. Sci.*, 2007, **253**, 9124–9129.
42 J. P. Sullivan, T. A. Friedmann and A. G. Baca, *J. Electron. Mater.*, 1997, **26**, 1021–1029.
43 Y. Lifshitz, G. D. Lempert, E. Grossman, I. Avigal, C. Uzan-Saguy, R. Kalish, J. Kulik, D. Marton and J. W. Rabalais, *Diamond Relat. Mater.*, 1995, **4**, 318–323.
44 D. W. MLau, D. G. McCulloch, N. A. Marks, N. R. Madsen and A. V. Rode, *Phys. Rev. B: Condens. Matter Mater. Phys.*, 2007, **75**, 233408.
45 J. Robertson, *Mater. Sci. Eng., R*, 2002, **37**, 129–281.